

Crystal structure of an acetylcholinesterase–fasciculin complex: interaction of a three-fingered toxin from snake venom with its target

Michal Harel¹, Gerard J Kleywegt², Raimond BG Ravelli^{3,4},
Israel Silman^{4,5} and Joel L Sussman^{1,4*}

¹Department of Structural Biology, Weizmann Institute of Science, Rehovot 76100, Israel, ²Department of Molecular Biology, Biomedical Centre, Uppsala University, Box 590, S-751 24 Uppsala, Sweden, ³Department of Crystal and Structural Chemistry, Bijvoet Center for Biomolecular Research, Padualaan 8, 3584 CH Utrecht, The Netherlands, ⁴Department of Biology, Brookhaven National Laboratory, Upton, NY 11973, USA and ⁵Department of Neurobiology, Weizmann Institute of Science, Rehovot 76100, Israel

Background: Fasciculin (FAS), a 61-residue polypeptide purified from mamba venom, is a three-fingered toxin which is a powerful reversible inhibitor of acetylcholinesterase (AChE). Solution of the three-dimensional structure of the AChE/FAS complex would provide the first structure of a three-fingered toxin complexed with its target.

Results: The structure of a complex between *Torpedo californica* AChE and fasciculin-II (FAS-II), from the venom of the green mamba (*Dendroaspis angusticeps*) was solved by molecular replacement techniques, and refined at 3.0 Å resolution to an R-factor of 0.231. The structure reveals a stoichiometric complex with one FAS molecule bound to each AChE subunit. The AChE and FAS conformations in the complex are very similar to those in their isolated structures. FAS is bound at the 'peripheral' anionic site of AChE, sealing the narrow gorge leading to the active site, with the dipole moments of the two molecules roughly aligned. The high affinity of FAS for AChE is due to a

remarkable surface complementarity, involving a large contact area (~2000 Å²) and many residues either unique to FAS or rare in other three-fingered toxins. The first loop, or finger, of FAS reaches down the outer surface of the thin aspect of the gorge. The second loop inserts into the gorge, with an unusual stacking interaction between Met33 in FAS and Trp279 in AChE. The third loop points away from the gorge, but the C-terminal residue makes contact with the enzyme.

Conclusions: Two conserved aromatic residues in the AChE peripheral anionic site make important contacts with FAS. The absence of these residues from chicken and insect AChEs and from butyrylcholinesterase explains the very large reduction in the affinity of these enzymes for FAS. Several basic residues in FAS make important contacts with AChE. The complementarity between FAS and AChE is unusual, inasmuch as it involves a number of charged residues, but lacks any intermolecular salt linkages.

Structure 15 December 1995, 3:1355–1366

Key words: α/β hydrolase fold, acetylcholinesterase, fasciculin, protein–protein complex, snake toxins

Introduction

The venoms of elapid snakes, including the Asian cobras and kraits, and the African mambas, contain a number of small proteins, 60–70 amino acid residues long, which display a broad spectrum of toxic activities [1]. Among the best studied are the α -neurotoxins of the venoms of kraits and cobras, such as α -bungarotoxin from the Formosan krait, *Bungarus multicinctus* [2], and the somewhat shorter α -cobratoxins isolated from the venoms of various cobras such as the Siamese cobra, *Naja naja siamensis* [3], both of which serve as potent and specific blockers of the nicotinic acetylcholine receptor [4]. Other toxins of this family serve as blockers of K⁺ channels and Ca²⁺ channels [5], as muscarinic receptor agonists [6] and as anticholinesterase agents [7]. Despite their diverse biological activities, these toxins display substantial sequence and structural homology. X-ray and NMR studies show that the toxins share a common structural motif: a core, containing four disulfide bridges, from which three loops protrude, roughly like the central fingers of a hand [8]. Accordingly, the family is known as the three-fingered toxin family [9]. Superposition of the structures of

different toxins reveals that, whereas the structure of the central core is conserved, the orientation of the fingers can vary considerably [5], suggesting that they serve as determinants of biological specificity. Until now, however, no three-dimensional structure has been available of a complex of a three-fingered toxin with its target.

Acetylcholinesterase (EC 3.1.1.7; AChE) is a synaptic enzyme the principal role of which is believed to be the termination of impulse transmission at cholinergic synapses by rapid hydrolysis of the neurotransmitter, acetylcholine (ACh) [10]. In accordance with its biological function, AChE possesses unusually high catalytic activity, especially for a serine hydrolase, functioning at a rate which approaches limitation by diffusion control [11]. Unexpectedly, the three-dimensional (3D) structure of AChE revealed that its active site is located near the bottom of a deep and narrow gorge, the surface of which is largely composed of the rings of an array of conserved aromatic amino acids [12]. Moreover, the so-called 'anionic' subsite, which is recognized by the quaternary group of the positively charged substrate, ACh, is not

*Corresponding author.

composed of a cluster of carboxylic groups, as was previously thought to be the case [13], but consists primarily of the rings of two of the conserved aromatic amino acids, Trp84 and Phe330. These residues are probably involved in electrostatic interactions with ACh through the π -electrons of their rings [14–16].

The existence of a second anionic site, known as the 'peripheral' site, was recognized many years ago, on the basis of the high affinity of the enzyme for bisquaternary ligands [17]. Various bulky ligands, such as the alkaloid *d*-tubocurarine, and the fluorescent probe propidium, inhibit AChE non-competitively by binding at this site [18]. Several lines of evidence suggest that the peripheral site is located at the top of the active-site gorge. Firstly, the layout of the active-site gorge [12]. Secondly, the crystal structure of a complex of *Torpedo* AChE with the bisquaternary inhibitor decamethonium [14]. And lastly, modeling studies of human butyrylcholinesterase (BuChE) [19], which is not susceptible to peripheral site inhibitors. Like the anionic subsite of the active site, conserved aromatic residues were postulated to play an important role in this site, in particular Tyr70, Tyr121 and Trp279 [12].

Electrostatic calculations reveal that the AChE molecule possesses a large dipole moment oriented in such a way that it would serve to attract the ACh down the gorge towards the active site [20]. The contribution of this field to the rapid turnover of AChE is the subject of substantial controversy [21–23].

Many of the toxins in the venoms of the elapid snakes are directed towards components of the cholinergic synapse, both presynaptic and postsynaptic [1,9]. It is, therefore, perhaps not surprising that one such toxin, fasciculin (FAS), is directed towards the synaptic enzyme AChE [7], resulting in severe, generalized and long-lasting fasciculations of skeletal muscle due to accumulation of increased levels of ACh within the synaptic cleft [24]. The three fasciculins described to date are 61-amino acid peptides, isolated from mamba venoms. They are potent reversible inhibitors of mammalian and electric organ AChEs, with inhibitory constant values of $\sim 10^{-11}$ – 10^{-12} M [25]. Fasciculins-I (FAS-I) and II (FAS-II), isolated and purified from the venom of the green mamba (*Dendroaspis angusticeps*), have been crystallized, and their structures determined to 1.9 Å [8] (PDB entry 1FAS) and 2.0 Å [26] (PDB entry 1FSC), respectively. These crystallographic studies revealed that, as predicted from the sequence similarities, they display strong structural homology with other three-fingered toxins [5,6,8,9].

The fact that the 3D structure of AChE [12] became available at about the same time as that of FAS-I [8] stimulated a wave of experimental studies aimed at elucidating the molecular basis for inhibition, using conventional enzyme kinetics [27–29], as well as chemical modification [25,30,31] and site-directed mutagenesis [29,32]. A theoretical study, in which docking of FAS onto the

AChE structure was attempted, has also been published [33]. Chemical modification suggested participation of a number of conserved basic residues of FAS in the interaction with AChE [25,30], and further suggested that the interaction took place at the peripheral anionic site of AChE, which is located at the mouth of the active-site gorge [31]. Site-directed mutagenesis has provided evidence for participation of aromatic residues from the peripheral site of mouse AChE (Tyr70, Tyr121 and Trp279) in the interaction with FAS [32]. A plausible mechanism for the mode of action of FAS would be blockage of the entrance to the active-site gorge, thus preventing access of the substrate to the active site. Recent studies suggest, however, that both substrates and inhibitors have access to the active site in the AChE/FAS complex [27–29]. Solution of the 3D structure of the AChE/FAS complex provides direct insight into the mode of action of FAS, as well as delineating the structural features, in both enzyme and toxin, which govern the specificity and potency of the interaction. Here we describe and analyze the 3D structure of a complex of *Torpedo* AChE with FAS-II.

Results and discussion

Description of the structure

The structure of the *Torpedo* AChE/FAS-II complex was solved and refined at 3.0 Å by standard crystallographic techniques. Details are given in the Materials and methods section and in Tables 1 and 2. Figure 1a shows an overview of the complex of the two proteins and Figure 1b shows the physiological dimer of the AChE/FAS-II complex. It is clear from Figure 1b that the two FAS molecules sit on opposite ends of the AChE dimer and do not interact with one another. Figure 2 shows a representative section of the final electron-density map.

The structures of both AChE and FAS-II in the complex are very similar to their structures in the uncomplexed forms. The root mean square deviation (rmsd) for 528 C α atoms in AChE, compared with the starting model for refinement [14], is 0.49 Å. Shifts greater than 1 Å occur for residues at the termini as well as for residues 281, 283, 333–337, 349–351 and 485. (Residue numbering for AChE here, and throughout the paper, is based on *Torpedo californica* AChE [34].) Apart from the termini, most of the shifted residues are in areas which form part of the AChE/FAS-II interface.

The rmsd for 61 FAS-II C α atoms is 0.79 Å, compared with the X-ray structure of the toxin alone [26], with shifts greater than 1 Å observed for some residues in the protein–protein interface (fingers I and II, residues 11, 12, 28–32), as well as for residues 19, 44 and 46.

As seen in Figure 1a, a large number of residues interact upon complex formation. The total loss of accessible surface area is ~ 2000 Å², at the top end of the scale observed for protein–protein hetero-complexes (excluding thrombin–inhibitor complexes) [35]. For comparison, in the

Table 1. Data collection and processing statistics.

Data set	1	2
Cell axes a, b, c (Å)	87.4, 115.0, 67.5	87.1, 116.8, 72.7
Diffraction limit (Å)	3.0	3.2
No. of observations	48 744	41 880
No. of independent reflections	14 206	12 382
Highest resolution shell (Å)	3.11–3.0	3.3–3.2
Completeness (%): all data	97.7	95.6
highest resolution shell	93.7	62.6
R _{sym} (on I)* (%): all data	10.5	5.9
highest resolution shell	30.3	32.3
I/σ(I): all data	10.7	18.8
highest resolution shell	3.5	3.3

*R_{sym}(I) = $\frac{\sum_{hkl} \sum_i |I_i(hkl) - \langle I(hkl) \rangle|}{\sum_{hkl} \sum_i I_i(hkl)}$, where $\langle I \rangle$ is the average intensity of the *i* observations of reflection *hkl*.

Table 2. Refinement and model statistics.

Resolution range (Å)	8.0–3.0
Number of reflections (F>0)	12 579
R-factor*	0.231
Last-recorded value of R _{free} [†]	0.315
No. of protein atoms (532+61 residues; Z>1)	4690
No. of hetero atoms (carbohydrate, water, 2 Zn ²⁺ ions)	52
Temperature factors (grouped one B per residue)	
Average B-factor for all protein atoms (Å ²)	19.5
Geometry: rms deviations from ideal values [53,61]	
Bond lengths (Å)	0.008
Bond angles (°)	1.4
Dihedral angles (°)	24.0
Improper torsion angles (°)	1.2
Ramachandran plot (non-Gly, non-Pro residues) [64]	
Residues in most favored regions (%)	81.9
Residues in additional allowed regions (%)	16.7
Residues in generously allowed regions (%)	1.0
Residues in disallowed regions (%)	0.4
Structural quality	
Residues with unusual peptide orientations (%) [54]	2.7
Residues with non-rotamer side-chain conformations (%) [54]	11.5
Residues with poor density (real-space R-factor>0.40) (%) [54]	2.4
Overall G-factor [64]	+0.23
Overall DACA score [65]	-1.00

*R-factor = $\frac{\sum_{hkl} | |F_{obs}(hkl)| - |F_{calc}(hkl)| |}{\sum_{hkl} |F_{obs}(hkl)|}$, where *F*_{obs}(*hkl*) and *F*_{calc}(*hkl*) are the observed and calculated values, respectively, for structure factor *hkl*. [†]R_{free} is equivalent to R-factor for a randomly selected 7% subset of reflections not used in structure refinement.

complex between Fab HyHEL5 and lysozyme (PDB entry 3HFL) ~1700 Å² of surface area are buried; in the barnase–barstar complex (PDB entry 1BGS), ~1600 Å²; in the subtilisin–eglin complex (PDB entry 1CSE), ~1500 Å² and in the complex of trypsin with bovine pancreatic trypsin inhibitor (PDB entry 1BRB), ~1400 Å². All these calculations of buried surface utilized a 1.4 Å probe radius [35].

The AChE/FAS-II interface can be divided roughly into three regions, which we denote A, B and C (see Table 3 and Figs 2,3).

Interface regions between AChE and FAS

Region A consists of residues 68–90 in AChE (i.e. the ω loop [36] which contains residues belonging to both the anionic site and the peripheral site) and loops I and II of FAS. Loop I of FAS is held in a vice-like grip by AChE. It interacts with the outer face of the thin aspect [36] of the active-site gorge (Asn85) which has the anionic site on its inner face (near Trp84), and with residues at the top of the gorge within the peripheral site (Tyr70 and Val71) (see Figs 2,3a). Contacts in this region involve only hydrophobic interactions and main-chain to side-chain hydrogen bonds.

Region B comprises residues 272–289 in AChE (corresponding to part of the peripheral site [14]). These residues interact predominantly (but not exclusively) with the second finger of FAS via polar interactions, several main-chain to side-chain hydrogen bonds, and additional hydrophobic interactions. Interestingly, one residue in FAS, Thr8, interacts both with Val71 (in region A) and Asp276 (in region B) (see Figs 2, 3a and 3b). The carboxylate oxygen atoms of Asp285 are within hydrogen-bonding distance of the backbone atoms of Pro30 in FAS, suggesting that this aspartate is protonated.

The most striking hydrophobic interaction is the stacking between the side chains of Met33 in FAS and Trp279 in AChE (Fig. 3b): the Sδ–Cε moiety of Met33 stacks parallel to the indole ring of the tryptophan, with the sulfur atom positioned roughly above the six-membered ring and the methyl group above the five-membered ring. Although such stacking interactions are rare, they are not unknown. For instance, in AChE itself, Met83 stacks in a similar way with Trp84 in the anionic site. A search of the PDB using SPASM (GJK, unpublished program) revealed other proteins in which a methionine and a tryptophan residue interact in a similar way. Examples include glucose oxidase (Trp131–Met268; PDB entry 1GAL), guinea fowl egg-white lysozyme (Trp28–Met105; PDB entry 1HHL), renin (Trp299–Met194; PDB entry 1RNE), and deoxy-hemoglobin (Trp130–Met114; PDB entry 2HBG).

Residues 279–284 in region B have relatively poor density in the 3.0 Å 2F_o–F_c map. However, in the 3.2 Å and cross-crystal averaged map it is shown unambiguously that both the main-chain trace and the side-chain orientations for this region are essentially correct.

Region B also contains a crystal packing artifact between AChE and FAS, namely the formation of a zinc-binding site (zinc being part of the crystallization liquor) in which the zinc ion is coordinated by Asp285 in AChE, His29 in FAS, and Glu49 from a symmetry-related copy of the AChE molecule. It is possible that the histidine and the aspartate would form an additional side-chain to side-chain hydrogen bond under physiological conditions (in the absence of zinc).

Region C comprises residues 334–358 in AChE (at the top of the gorge, see Fig. 1a). This region has a few

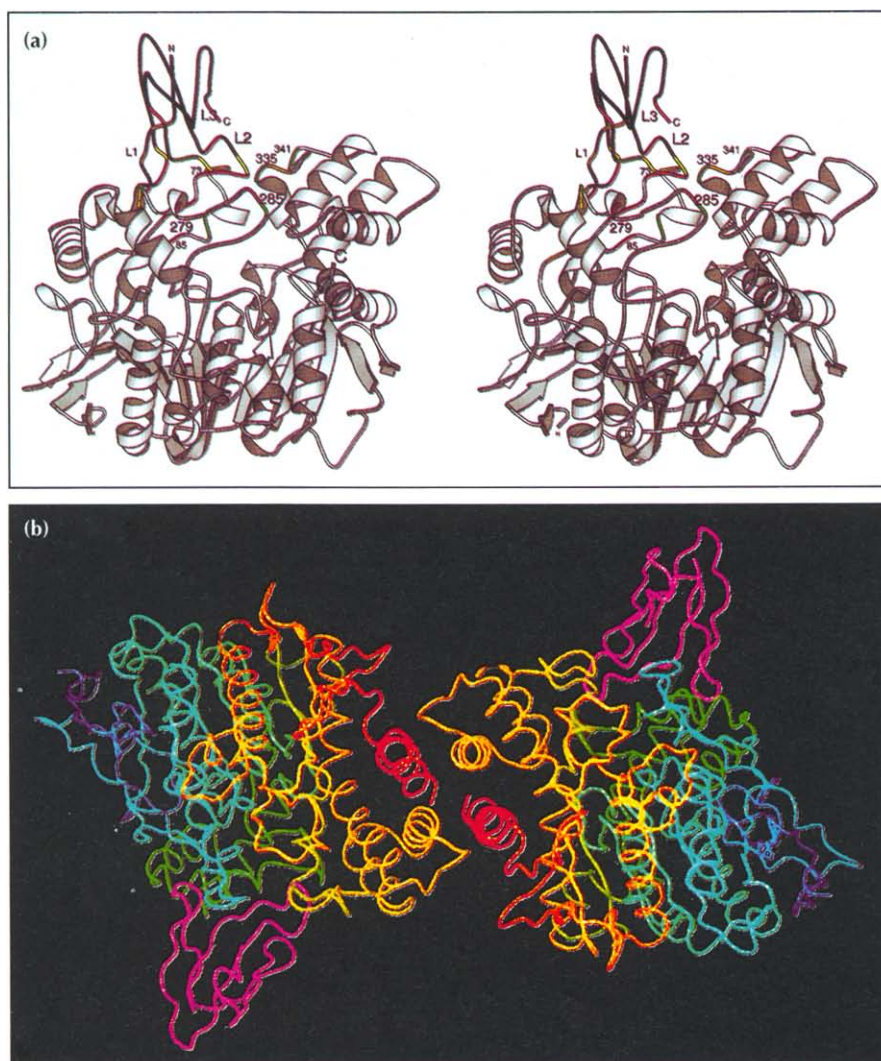


Fig. 1. AChE/FAS-II complex. (a) Stereo ribbon drawing of AChE (grey) and FAS-II (black) showing the interactions between them. Residues which participate in hydrophobic interactions are green, those involved in hydrogen bonds are yellow, and those participating in both kinds of interaction are red. L1, L2 and L3 denote loops I, II and III, respectively. (b) Physiological dimer of AChE/FAS-II complexes. The AChE molecules are color-ramped from blue at their N termini to red at their C termini. The FAS molecules are shown in magenta.

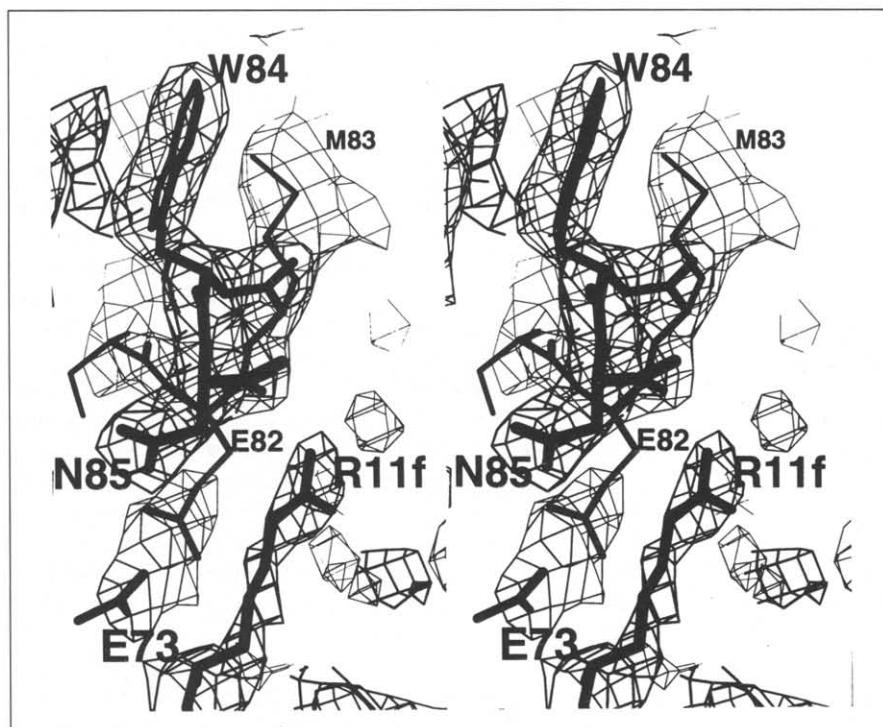


Fig. 2. Representative portion of the final $3F_o - 2F_c$ map of the AChE/FAS-II complex for part of interface region A. It shows the interaction between Asn85 (AChE) and Arg11 (FAS-II). The segment Glu82-Asn85 of AChE is displayed. In addition, the unusual carboxylate interaction between Glu73 and Glu82 in AChE is shown.

Table 3. Surface accessibilities and interactions of residues at the AChE/FAS-II interface.

Residue	B-factor (Å ²)	Surface loss (Å ²)*	Hydrogen bonds (Å)	Hydrophobic interactions (Å)	Residue	B-factor (Å ²)	Surface loss (Å ²)*	Hydrogen bonds (Å)	Hydrophobic interactions (Å)
Region A					Region B (continued)				
Tyr70	3.7	64 (4)	OH-Val34 O (3.2)	Cδ1-Thr8 Cγ2 (3.7)	Asn280	14.6	27 (55)		
Val71	24.5	53 (4)	N-Thr8 O (2.9)	Cε1-Thr8 Cγ2 (3.9)	Leu282	41.7	42 (14)		Cδ1-Arg27 Cζ (3.7)
				Cγ1-Arg11 Cγ (4.0)					Cδ1-Pro31 Cδ (3.8)
				Cγ2-Thr9 Cα (3.7)					Cδ1-Pro31 Cγ (3.8)
				Cγ2-Thr9 C (3.6)	Asp285	39.7	60 (54)	Oδ1-Pro30 N (3.2)	Cγ-His29 Cβ (3.6)
Glu73	22.1	84 (0)	O-Arg37 Nη1 (2.8)	Cβ-His6 Cδ2 (3.7)			Oδ1-Pro30 O (3.0)		
			O-Arg37 Nη2 (2.7)	Cβ-His6 Ce1 (3.6)	Ser286	19.0	40 (4)	N-Pro30 O (3.1)	
				Cγ-His6 Cδ2 (3.9)	Arg289	2.0	5 (36)		
				Cγ-Ala12 Cβ (3.8)					
				Cδ-Arg11 Cα (3.8)	Region C				
				Cδ-Ala12 Cβ (3.8)	Tyr334	10.5	67 (19)	O-Lys32 N (2.6)	
				Cδ-Ala12 Cβ (3.2)	Gly335	42.7	47 (16)		
Gln74	14.0	62 (15)		Cα-Tyr61 Cζ (3.9)					Cα-Lys32 Cγ (3.8)
Phe75	12.4	18 (17)		Cδ-Arg37 Cζ (4.0)					Cα-Lys32 Cδ (3.8)
Pro76	12.4	93 (10)		Cδ-Tyr61 Cδ2 (4.0)	Lys341	19.1	12 (31)	Nζ-Tyr61 Oη (3.0)	C-Pro30 Cγ (3.9)
				Cδ-Tyr61 Ce2 (3.9)	Asp342	32.8	11 (109)		
				Cβ-Tyr4 Cδ1 (4.0)	Leu358	32.8	14 (22)		
				Cβ-Tyr4 Ce1 (3.9)	FAS-II				
				Cβ-Ala12 Cβ (3.9)	Tyr4	10.0	16 (24)		
				Cγ-Arg37 Cζ (3.3)	His6	2.0	15 (12)		
Glu82	23.6	33 (18)	O-Arg11 Nη2 (2.9)	Cβ-Arg11 Cζ (4.0)	Thr7	6.5	9 (69)		
Asn85	9.6	10 (8)	O-Arg11 Nη2 (3.6)		Thr8	2.0	97 (1)		
Pro86	15.9	9 (12)			Thr9	10.0	107 (27)		
Asn87	2.0	10 (70)		Cε-Thr9 Cβ (3.6)	Ser 10	20.1	16 (38)		
Met90	2.0	26 (46)			Arg11	22.6	124 (104)		
Region B					Ala12	12.3	31 (23)		
Gln272	23.9	21 (76)		Cβ-Thr8 Cγ2 (4.0)	Arg24	2.0	13 (38)		
Ile275	10.4	21 (1)		Cγ2-Thr8 Cβ (3.9)	Arg27	2.0	73 (26)		
				Cγ2-Thr9 Cγ2 (4.0)	His29	14.6	22 (85)		
				Cδ1-Thr9 Cγ2 (3.3)	Pro30	6.6	85 (11)		
Asp276	53.8	51 (67)	Oδ1-Thr8 Oγ1 (2.6)		Pro31	2.0	68 (15)		
			Oδ2-Thr8 Oγ1 (3.6)	Cβ-Met33 Sδ (3.6)	Lys32	22.7	49 (85)		
Trp279	53.8	67 (9)	O-Arg27 Nη1 (2.8)	Cγ-Met33 Sδ (3.1)	Met33	17.8	83 (5)		
				Cδ2-Met33 Sδ (3.2)	Val34	7.2	40 (0)		
			Cδ2-Met33 Ce (3.7)	Ce2-Met33 Sδ (3.7)	Leu35	5.9	31 (23)		
				Ce2-Met33 Ce (3.7)	Arg37	15.1	29 (4)		
				Ce3-Met33 Sδ (3.7)	Asn47	49.8	22 (77)		
				Cδ1-Met33 Sδ (3.6)	Tyr61	25.0	100 (85)		
				Cζ2-Met33 Ce (3.9)					

Residues in AChE that lose more than 5 Å² of accessible surface area upon complex formation with FAS-II are listed together with their interactions with residues in FAS-II. For possible hydrogen bonds, a distance cutoff of 3.6 Å was used; for hydrophobic interactions, a distance cutoff of 4.0 Å was used. These rather high cutoff values were chosen to take into account the uncertainty in the atomic positions. *Loss of accessible surface area upon complex formation. The amount of exposed surface remaining in the complex shown in parentheses.

interactions with residues in loop II of FAS and with Tyr61 at the C terminus. Thus, FAS uses not only loops I and II, but also the C-terminal tyrosine (which is conserved in the fasciculins, but rare in other toxins) to interact with the top of the gorge of AChE.

In summary, the interface between AChE and FAS-II consists largely of hydrophobic interactions, together with three main-chain to main-chain hydrogen bonds, eight main-chain to side-chain hydrogen bonds, and only three polar side-chain interactions. The striking absence of salt links in the interface cannot be attributed to a lack of charged residues. Five acidic residues from AChE (Glu73, Glu82, Asp276, Asp285 and Asp342) and five basic residues from FAS-II (Arg11, Arg24, Arg27, Arg37 and Lys32) are found at the interface. Perhaps the pH of the crystallization solution (~5.2) also plays a role in determining the nature of interface contacts, inasmuch as

some of the acidic residues may well be protonated, thus favoring hydrogen-bonding interactions. In AChE, both Glu73 and Glu82 are probably protonated, as they form double hydrogen bonds through their carboxylate groups (Fig. 2). Asp276 and Asp285 are involved in hydrogen bonds with residues in FAS-II, and Asp285, in addition, coordinates the zinc ion mentioned earlier. Asp342 appears to have no hydrogen-bonding interactions in our structure. Of the basic residues in FAS, the amino group of Lys32 has no apparent hydrogen-bonding interactions. Three of the four arginine residues (Arg11, Arg27 and Arg37) form hydrogen bonds with atoms in AChE. The Nε atom of Arg24 forms an internal hydrogen bond to Oγ of Ser26 in FAS; in addition, its guanidino Nη1 atom forms an internal salt link with the C-terminal carboxyl group of Tyr61. Arg27 appears to play a role in orienting or stabilizing the Pro-cis-Pro turn in finger II: its Nε atom is within hydrogen-bonding distance of the

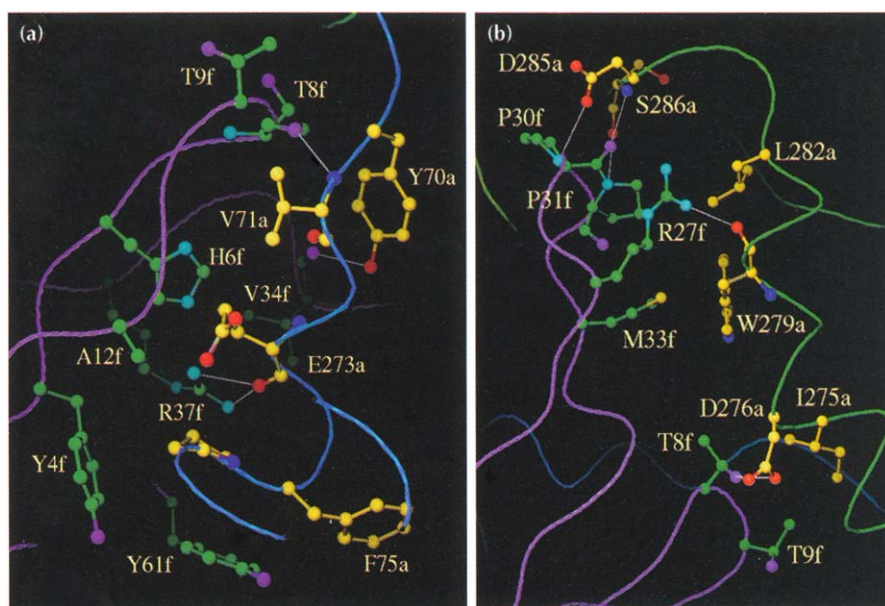


Fig. 3. Details of the AChE/FAS-II interface with interacting residues shown as ball-and-stick models. The letters 'a' or 'f' after the residue number refer to AChE and FAS-II, respectively. **(a)** Region A covering AChE residues 68–90, showing the large number of hydrophobic interactions. **(b)** Region B, covering AChE residues 271–289.

carbonyl oxygen atoms of His29 and Pro31, whereas its guanidino N η 1 atom forms a hydrogen bond with the carbonyl oxygen of Pro30.

There exists a remarkable shape complementarity between AChE and FAS-II in the interface. Figure 4 shows how the first two fingers of FAS fit snugly into depressions in the surface of AChE near the mouth of the gorge. This figure also suggests that FAS blocks the entrance to the gorge. This is confirmed by volume calculations as shown in Figure 5. Without bound FAS, the gorge is connected to the external solvent (i.e. accessible to a probe with a radius of 1.4 Å), but in the complex the entrance is sealed.



Fig. 4. Complementarity of the surfaces of AChE and FAS-II in their complex. The coloring scheme for AChE and FAS-II is the same as in Figure 1b. The semi-transparent van der Waals surface of AChE is shown in blue.

For the reasons outlined below, we are confident that the interface described here is the one existing under physiological conditions. However, due to crystal packing there are additional interactions between AChE and FAS-II, as well as between symmetry-related FAS molecules. The symmetry contacts between AChE and FAS-II (in addition to those involving the zinc ion mentioned earlier) involve a few hydrophobic and polar interactions between a limited set of residues: Glu49, Pro50, Arg174, Met175, Gln178 and Gly214 in AChE, and His29, Gly44, Asp45, Asp46 and Asn47 in FAS-II.

Theoretical docking studies by van den Born *et al.* [33] produced a set of three models for the AChE/FAS complex. For each model, a set of possible electrostatic, hydrophobic and polar interactions was listed. Of the hydrophobic contacts listed, none are observed in our crystal structure, and only one polar interaction actually corresponds to an observed hydrogen bond (Glu73 in AChE to Arg37 in FAS, which they proposed in their model complex #58; the other six polar interactions listed for this complex do not occur). Because many models were generated, but only a few were chosen for further scrutiny, selection of those models may well have been driven by the anticipation of electrostatics-driven complex formation.

Specificity of interaction

The structure we have determined clearly demonstrates that, as predicted [32], FAS-II inhibits *Torpedo* AChE by binding at the top of the active-site gorge, overlapping the peripheral anionic site. However, the FAS orientation does not conform to any of those predicted by docking studies [33]. The FAS-II molecule makes contact through its first two fingers, that is loops I and II, with loop III actually pointing away from the AChE molecule.

A principal point to be emphasized is that there is little difference in the overall conformations of either FAS-II

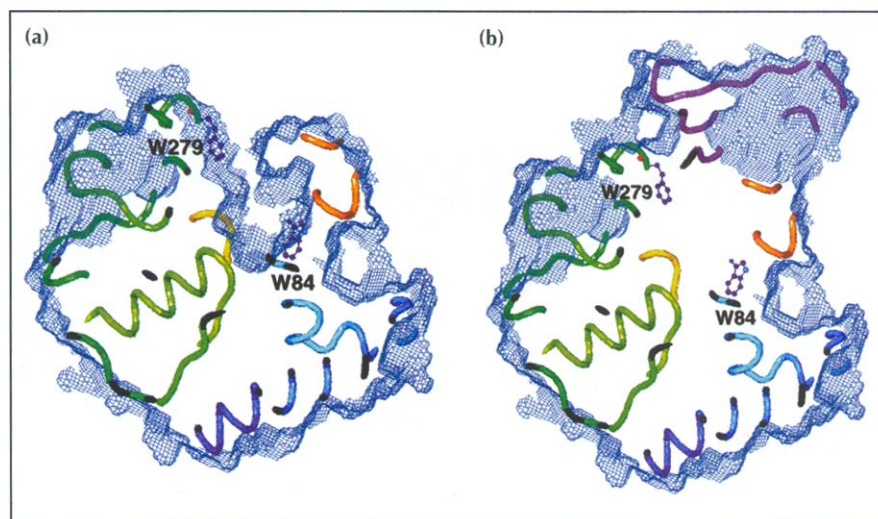


Fig. 5. A slice through the active-site gorge of AChE. The bottom of the gorge is indicated by Trp84 (ball-and-stick) and the peripheral site by Trp279. The coloring scheme for AChE and FAS-II is the same as that in Figure 1b. (a) AChE alone — the gorge is accessible to external solvent. (b) The AChE/FAS-II complex, with the gorge blocked by FAS-II.

or *Torpedo* AChE in the complex relative to their native structures. The high affinity observed must, therefore, result from a high degree of complementarity. This, in turn, arises from a rather large contact area, as well as involvement in the interface of a substantial number of residues either unique to the fasciculins, or occurring only rarely in other members of the three-fingered toxin family (Fig. 6). The crystal structures of FAS-I and FAS-II are very similar. They have an rmsd of 0.6 Å for 53 out of 61 C α atoms; this excludes the first finger (residues 6–13), which is in a markedly different conformation in the crystal structures of FAS-I and FAS-II (up to 10 Å difference). In the crystal structure of FAS-I, this region has relatively high temperature factors [8], and was shown to be flexible in a number of three-fingered toxins in solution [5]. If FAS-I were placed, as a rigid body, in the position and orientation of FAS-II in the complex, loop I would clash with residues 72–77 of AChE. Because the sequences of FAS-I and FAS-II are virtually identical (the only change is Tyr47→Asn), and the two toxins bind to AChE with similar affinity, it is likely that FAS-I adopts a very similar conformation to that of FAS-II when complexed with AChE.

AChEs of fish and mammals, but not BuChEs, are susceptible to inhibition by FAS. Several insect, bird and reptile AChEs are, however, poorly inhibited by FAS. The present model of the AChE/FAS complex, combined with alignments of various esterase sequences,

provides hints as to the identity of the residues in AChE that are responsible for this inhibition (Fig. 7). Clearly, key residues which are responsible for affinity, or lack thereof, must be buried in the complex, must not be identical in BuChE and AChE, and are probably strictly conserved in the susceptible AChEs. Figure 7 shows that only residues 70, 71 and 279 strictly satisfy all these criteria. In BuChEs, Val71 is replaced by isoleucine, which is a conservative substitution, but Tyr70 is replaced by asparagine and Trp279 by arginine, alanine or valine. These non-conservative changes at positions 70 and 279 are bound to interfere with, or preclude, the favorable hydrophobic interactions in which these two residues are involved in the AChE/FAS complex.

Role of aromatic residues

Site-directed mutagenesis of mouse recombinant AChE pointed to an important role for three conserved aromatic residues, namely Tyr70, Tyr121 and Trp279, in the interaction with FAS-II [32]. All three are located near the top of the gorge, with their aromatic rings pointing into it, and have been assigned to the peripheral site also on the basis of their involvement in interactions with other peripheral-site-specific inhibitors [19,37–40]. Our 3D structure shows that two of these residues, Tyr70 and Trp279, interact with residues in FAS-II. The third residue, Tyr121, is not in direct contact with FAS-II; it is located inside the gorge and is surrounded by six other aromatic residues. A role for this residue in the binding



Fig. 6. Comparison of the amino acid sequences of fasciculins (FAS-I, FAS-II and FAS-III) with 163 other non-FAS toxin sequences that are found in the SWISS-PROT database [68]. Residues that occur in the fasciculins but do not occur in that position in any of the other toxins are indicated in red; those that are rarely found in other toxins (occurring in five or fewer of these sequences) are in bold. The amino acids that make up the three fingers are underlined. Asterisks indicate those residues that lose more than 5 Å² of accessible surface area in the complex with AChE. The fasciculins and other toxins were aligned using the PILEUP program [69] of the GCG package (Genetics Computer Group, Madison, Wisconsin).

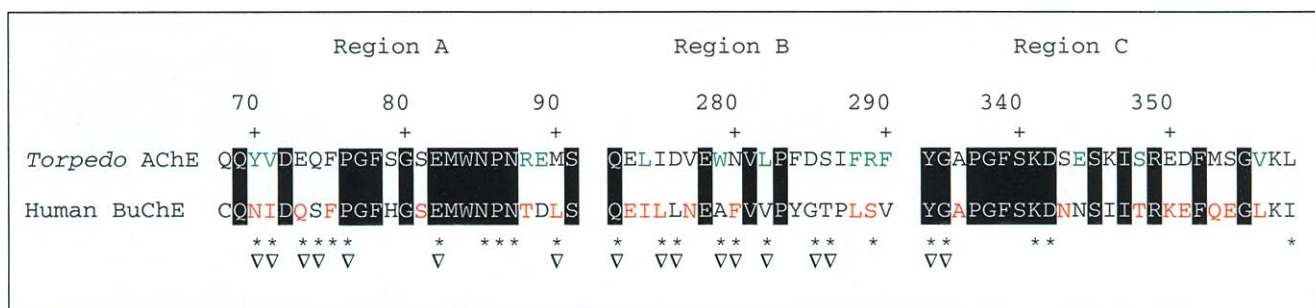


Fig. 7. Comparison of the amino acid sequences of *Torpedo* AChE and human BuChE with all other sequenced AChEs and BuChEs in the three regions of AChE that interact with FAS in the complex. The AChE and BuChE sequences were taken from the 'ESTHER' server [70] (URL: <http://www.montpellier.inra.fr:70/1/cholinesterase>). White text indicates residues conserved in both AChEs and BuChEs; residues conserved in AChEs only are indicated in green and those conserved in BuChEs only are in red; asterisks indicate AChE residues interacting with FAS, and triangles mark residues that lose more than 20 Å² of accessible surface area upon binding FAS.

site for the toxin was assigned on the basis of the Tyr121→Gln mutation, which reduced affinity towards FAS ~100-fold [32]. However, mutation of the corresponding residue to alanine, in human recombinant AChE, slightly increased affinity for the peripheral-site ligand, propidium [40]. The introduction of a polar glutamine residue into the aromatic cluster lining the wall of the gorge probably has an indirect effect on the geometry of the binding site for FAS.

Participation of Tyr70 and Trp279 in the binding site for FAS-II of *Torpedo* AChE is also in agreement with the fact that these two residues, as well as Tyr121, are not conserved in BuChE, which shows a low affinity for FAS, as well as for the low molecular weight peripheral-site ligands [7,24,32]. It was elegantly demonstrated [32] that production of a triple mutant in mouse AChE, in which the residues equivalent to *Torpedo* Tyr70, Tyr121 and Trp279 were replaced by asparagine, glutamine and arginine, respectively, reduced its affinity for FAS by eight orders of magnitude, to a value very similar to that observed for wild-type BuChE. The affinity for FAS for the double mutant, in which only the two residues equivalent to Tyr70 and Trp279 in *Torpedo* were mutated, was only slightly greater. Furthermore, as already mentioned, the AChEs of insect, avian and reptile species all display reduced affinity for FAS [7]. *Drosophila* AChE lacks all three of the conserved aromatic residues at the top of the gorge [41], and chicken AChE lacks both Tyr70 and Trp279 [39], whereas AChE purified from the venom of *Bungarus fasciatus* (X Cousin *et al.*, personal communication) lacks only Tyr70. It is interesting that in *B. fasciatus* AChE, Asp285 is substituted by lysine. When this lysine is replaced by aspartate, by site-directed mutagenesis, the affinity for FAS and peripheral-site ligands is substantially increased (X Cousin *et al.*, personal communication). This is in agreement with the observed interaction of Pro30 with Asp285 and our prediction of an interaction between His29 and Asp285 (see above) in the AChE/FAS-II complex under physiological conditions.

Comparison of the sequences of the three known fasciculins with those of 163 other toxins reveals that a

number of residues which are involved in the interface with AChE are unique to the fasciculins or are rarely found in other toxins (Fig. 6). Based on the alignment, Met2, Thr7, Pro30, Pro43 and Pro56 are unique. Other interface residues occur in very few non-FAS toxin sequences (the number of sequences, out of 163, in which these residues occur is shown in parentheses): Thr1 (4), Thr9 (4), Arg11 (4), Ala12 (4), Leu14 (1), Asn16 (5), Arg24 (5), Arg27 (1), His29 (1), Met33 (2), Leu35 (5), Gly36 (2), Gly44 (2), Asp46 (1), Asn47 (4), Leu48 (3) and Tyr61 (1). This includes six of the seven residues in FAS-II that lose the most accessible surface area upon complex formation and excludes Thr8, which is found in 32 non-FAS toxin sequences. The seven residues, in descending order of surface loss, are numbers 11, 9, 61, 8, 30, 33 and 27 (see Table 3). Pro56 is a deletion in all other sequences; perhaps this residue is required to orient the C terminus properly.

Role of basic residues

We have identified several critical basic residues within the FAS molecule. Their key roles are in agreement with earlier predictions made on the basis of the 3D structure of FAS-I coupled with the effects of chemical modifications on the toxin's biological activity. Thus, both acetylation of Lys32 and Lys51, and modification of Arg11 and Arg27, greatly reduced the potency of FAS [25,30]. Of these four basic residues, Arg11 and Arg27 occur only rarely in other three-fingered toxins. As detailed above (see Table 3), three of these residues make important contacts in the AChE/FAS complex: Arg11 in FAS with Asn85 and Val71; Arg27 with Trp279; and Lys32 with Tyr334. Arg27 also stabilizes the turn 29–31 in FAS. There is no structural evidence for involvement of Lys51 of FAS in the interaction with AChE. It is possible that its modification could perturb contacts between loops III and II, and thus, indirectly, interaction of loop II with AChE.

Role of electrostatic forces

It has been noted previously that AChE has a large dipole moment (~1700 Debyes) aligned approximately along the axis of the active-site gorge [20,22,36,42]. The field due

to this dipole might actually draw the positively charged substrate, ACh, towards and down the gorge to the active site. Similarly, FAS-II has its charges separated (dipole moment of ~ 185 Debyes), with most basic residues occurring in the first two fingers, and most acidic residues in the third finger [24,33] (Fig. 8). As the first two fingers make up most of the interface with AChE, and the third finger lies away from AChE, visual inspection suggests that the dipole moments of both proteins are roughly aligned in the complex. Indeed, electrostatic calculations [43,44] show that the angle between the dipole vectors of the two proteins is only $\sim 30^\circ$ (see Fig. 9) (C Felder, personal communication).

A priori, a reasonable mode of action of FAS, based on the static crystal structure which we have described and analyzed, would involve physical blocking of the mouth of the active-site gorge, thereby preventing access of substrate to the active site. Indeed, surface calculations, using a 1.4 Å probe radius, show that not even a water molecule would be able to penetrate the gorge in the crystal structure of the complex. Kinetic data suggest, however, that in solution, FAS does not completely seal off the active site from the bulk solution. The stoichiometric complex is still capable of reacting with organophosphate inhibitors [27], and displays residual catalytic activity

[28,29]. In the Trp84→Ala mutant of mouse AChE, binding of FAS actually enhances the rate of hydrolysis of neutral esters [29]. The 3D model of the AChE/FAS complex may provide a structural explanation for such an allosteric effect, as the bound FAS-II molecule actually spans the ω loop (residues 68–94). This loop is homologous to the ‘lid’ of the neutral lipases which, like AChE, are members of the α/β hydrolase fold family [45,46]. Thus, FAS makes contact not only with Tyr70 and Trp279 in the peripheral site, but also stretches down the outside of the thin aspect of the gorge to make contact, via Arg11, with Asn85, which lies adjacent to Trp84, the key residue of the anionic subsite of the active site.

However, the crystal structure of the AChE/FAS complex provides no clue as to the route by which substrates and inhibitors, whether charged or neutral, penetrate to the active site. This enigma is reminiscent of that encountered in the crystal structure of the native enzyme. Although the entrance to the active-site gorge appeared to be completely blocked by a symmetry-related subunit in the crystal structure [36], no difficulty was experienced in soaking several ligands into the native crystals [14,15]. Thus, the transition-state analog, *m*-(*N,N,N*-trimethylammonio)trifluoroacetophenone (TMTFA) [47], could be soaked into crystals of native *Torpedo* AChE, and the

Fig. 8. Isopotential electrostatic surface looking straight into the active-site gorge of AChE, contoured at ± 1 kT e^{-1} . Negative surface potential is shown in red and positive in blue. (a) AChE alone showing the deep gorge, with red surface over the gorge. (b) AChE/FAS-II complex showing FAS-II covering the gorge.

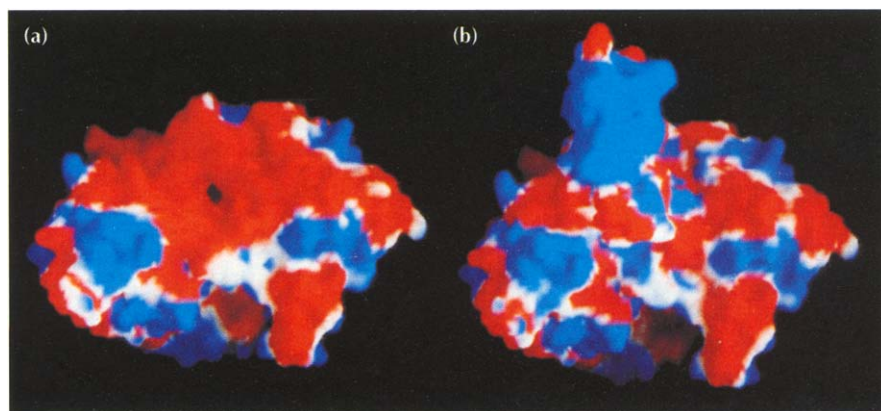
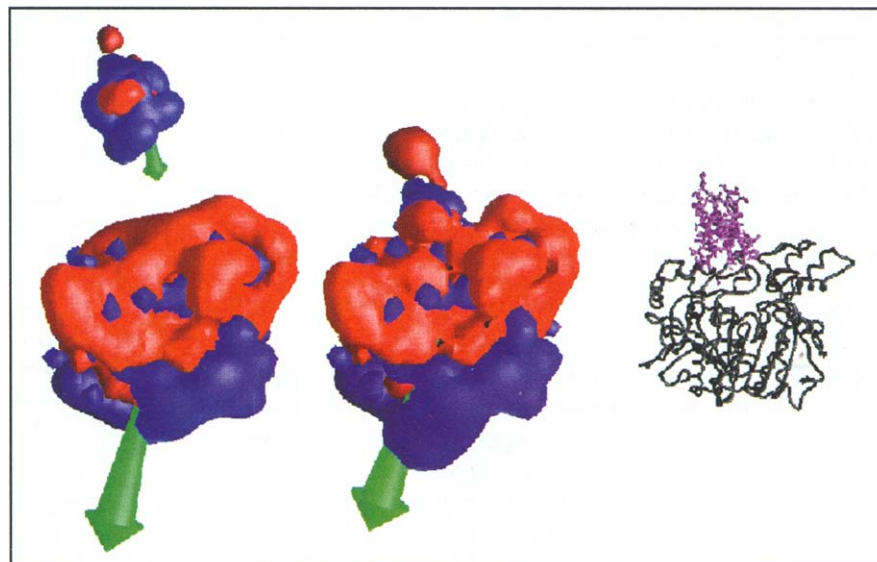


Fig. 9. Electrostatic potential with dipole moments drawn showing the attraction of FAS-II (top left) to AChE (bottom left) and the complex of AChE/FAS-II (right). The calculations were made assuming a pH of 7.0 and physiological ionic strength. The $C\alpha$ trace of the structure of AChE and FAS-II, drawn to the same scale, is shown on the right.



structure of the complex so obtained was solved [15]. However, in a preliminary experiment, a data set collected on a crystal of the AChE/FAS complex which had been exposed to 2 mM TMTFA for six days, revealed no TMTFA within the active site (data not shown). Grochulski and coworkers [48] have solved 3D structures of neutral lipases in which the lid was either open or shut. We must, therefore, face the possibility that the crystal structures of both native AChE and the AChE/FAS complex do not faithfully reflect the situation in solution. 'Back doors' or 'side doors' may exist through which traffic of substrate, products and water may occur [49], either permanently or transiently.

Biological implications

Acetylcholinesterase (AChE), the enzyme which hydrolyzes the neurotransmitter acetylcholine, is inhibited selectively by some snake venom toxins. Because of the relatively large size of these toxins (60–70 residues), they are not expected to penetrate the deep and narrow gorge leading to the active site of AChE but to inhibit it by binding at its so-called 'peripheral' site.

We have determined the three-dimensional structure of a 1:1 complex between *Torpedo californica* AChE and fasciculin-II (FAS-II), a three-fingered toxin from the venom of the green mamba, *Dendroaspis angusticeps*. In conjunction with mutagenesis data, this has enabled us to propose a model for the toxin's mode of action and the inhibitory interactions at the peripheral site. Indeed, the structure of the complex reveals physical blocking of the entrance to the AChE active-site gorge by FAS-II. However, the static crystal structure does not explain the fact that, in solution, the complex reacts with organophosphate inhibitors and displays residual catalytic activity.

The high affinity of FAS for AChE can be attributed to a remarkable surface complementarity, involving an unusually large contact area (~2000 Å²) and many residues either unique to FAS or rare in other three-fingered toxins. Several basic residues in FAS make important contacts with AChE. Another striking feature is the lack of intermolecular salt linkages at the AChE/FAS interface. The two proteins also have large dipole moments, that are roughly aligned in the complex, suggesting that electrostatic forces may be guiding the interaction.

Obviously, the generality of our findings with respect to the mode of interaction of other three-fingered toxins with their targets cannot be easily assessed as long as the structure of the AChE/FAS-II complex is the only one available. Although the three-dimensional structures of FAS-II and AChE separately and in their complex

are very similar, the flexibility of the structure of the three-fingered toxins means that substantial conformational change could occur upon complexation of a given toxin with its target. Albrand and coworkers [5] have analyzed the structural differences between FAS-II and the Ca²⁺ channel blocking FS2 toxin from black mamba venom. In particular, these authors have suggested that replacement of two aspartate residues in loop III of FAS-II by hydrophobic residues in the FS2 toxin, deprives the latter of the dipole character of FAS-II, and could help to explain why FS2 does not display anticholinesterase activity. Overall, it is likely that the flexibility of the three-fingered toxin structure will result in a large area of surface complementarity between toxin and target, leading to high specificity and high affinity.

Materials and methods

Crystallization

Single crystals of AChE/FAS-II were grown by the vapor diffusion method at 4°C using 20–25% PEG 200, 0.1 M sodium acetate buffer (pH 5.2), and 0.001 M zinc acetate in the reservoir. The 3 µl drops contained a 1:1 ratio of protein and reservoir. The AChE/FAS-II solution contained a 1:1 stoichiometric mixture of *Torpedo* AChE (13 mg ml⁻¹) and FAS-II (2.3 mg ml⁻¹). FAS-II was purified from *Dendroaspis angusticeps* venom by Alomone Labs (Jerusalem, Israel). Crystals belonging to space group P2₁2₁2 appeared overnight and grew, in a few days, to a size of 0.3 mm×0.15 mm×0.15 mm.

Data collection

Data were collected at 90 K using the Brookhaven National Laboratory NSLS beamline X12C, at 1.15 Å, with a 30 cm MAR image plate scanner. Two data sets were collected using crystals with up to 7% differences in cell dimensions. Due to these differences, the two data sets merged poorly (R_{merge} ~29%) and were, therefore, kept separate for refinement and map averaging. Data processing, scaling and merging was carried out with DENZO and SCALEPACK [50].

Structure solution and refinement

The structure was solved by molecular replacement [51] using the program AMORE [52], starting from the 2.3 Å refined structure of native AChE (MH, unpublished data). Both data sets yielded a single clear solution; after rigid-body refinement, the R-factors were 42% and 46%, and the correlation coefficients were 0.57 and 0.52 for data sets 1 and 2, respectively.

Refinement using X-PLOR [53], based on the AChE structure alone, resulted in the R-factor initially dropping from 48.5% to 26.3% for F>1σ data. The F_o-F_c map at 2.5σ showed the possible location of FAS-II. The structure of FAS-I (PDB entry 1FAS) was fitted into this density. After rebuilding with O [54], it was noted that loop I of FAS had undergone a major change, with a maximum shift of 10.5 Å for residue 9 at its tip. Enhancement of the FAS portion of the map was achieved with the program DMmulti (K Cowtan, unpublished program), in the CCP4 program suite [55], which was used to average the density of the maps of data set 1 and data set 2. The averaged density confirmed that a major conformational change of loop I had indeed occurred (Cα rmsd 2.6 Å for all residues). At that time, the structure of FAS-II became available (PDB entry

1FSC) and was found to fit the rebuilt FAS-I molecule ($C\alpha$ rmsd 0.9 Å). However, the free R-factor was high (~39%) and several areas in the FAS structure had poor electron density.

In view of the difficulties encountered in refinement, the correctness of the model of the complex was assessed using a six-dimensional real-space rigid-body fitting procedure of a partial FAS-II model in a map calculated with phase information from the AChE alone (program ESSENS [GJK and TA Jones, unpublished program]). This procedure yielded one outstanding peak (~15 σ above the average score; next best peak ~9 σ).

The crystal structure of FAS-II was then oriented and positioned according to the best solution and rebuilt in the map calculated with AChE phases only. The 2.8 Å structure of AChE in complex with edrophonium (PDB entry 1ACK [14]), together with the rebuilt FAS-II structure, were used as the starting model for further refinement.

In view of the limited number of diffraction data [56], the model of the AChE/FAS-II complex was refined conservatively. Only one temperature factor per residue was refined, and, during simulated-annealing refinement [57], harmonic restraints were used to prevent artificial deviations from the (higher resolution) starting models. The free R-factor [58] was used throughout to monitor the progress of the refinement. In between refinement cycles, the entire model was checked and rebuilt carefully with O [54] and OOPS [59]. Besides conventional $2F_o - F_c$ and $F_o - F_c$ maps, systematic simulated-annealing omit maps were used in one rebuilding cycle (omitting 10 protein residues at a time), and an averaged $2F_o - F_c$ map (using cross-crystal averaging [60] with the 3.2 Å crystal form, data set 2) was used in the two final rebuilding cycles. Two zinc ions and a conservative number of water molecules (36) were included in the final model. In addition, one *N*-acetylglucosamine moiety has been modeled (attached to Asn59 in AChE). As in the native structure [12], residues 1–3, 536 and 537 in AChE were not observed in the density and are not included in the model. However, residue 535 (not seen in the native 2.8 Å structure) is observed and there is weak density for parts of the main chain for residues 486–491 (also not observed in the native AChE structure). Residues 486–491 have, therefore, been modeled as alanine residues.

The final model has a crystallographic R-factor of 23.1% for all data between 8.0 Å and 3.0 Å, the last-recorded value of the free R-factor, prior to the final minimization, was 31.5%, calculated using 975 reflections (~7%) of the data not used in the refinement. The stereochemistry was tightly restrained to ideal values [61]. There are only two outlier residues in the Ramachandran plot [62], both in AChE: Ser200 (the active-site serine, an outlier in all α/β hydrolase structures [46]) and Leu23. However, both residues have good density. Coordinates of the final model and experimental structure-factor amplitudes (for the 3.0 Å data set) have been deposited with the PDB [63] (ID codes 1FSS and 1FSS-SF, respectively).

Software

All map calculations were done with various programs in the CCP4 package [55]. Maps were averaged with programs in the RAVE package [60]. All refinement was carried out with X-PLOR [53], using the Engh and Huber [61] force field. All graphics operations, modeling and model building were done with O [54]. All models were subjected to critical quality checks with O, X-PLOR [53], PROCHECK [64] and WHAT IF [65]. Surfaces were calculated with VOIDOO [66].

Figure 1a was prepared with MOLSCRIPT [67], Figures 1b and 2–5 with O [54] and Figures 8 and 9 with GRASP [43,44].

Note added in proof

In an independent study, the crystal structure of the complex between mouse AChE and fasciculin-II has been determined (Bourne, Y., Taylor, P. & Marchot, P. [1995] *Cell* **83**, 503–512). A joint comparison of the coordinates of the two complexes should yield important information concerning the amino acid residues participating in the interaction between the toxin and the enzyme in both complexes.

Acknowledgements: This work was supported by the US Army Medical Research and Development Command under Contract DAMD17-93-C-3070, the Minerva Foundation, Munich, Germany, the Kimmelman Center for Biomolecular Structure and Assembly, Rehovot, Israel, the Israel Academy of Sciences, Uppsala University and the Swedish Natural Science Research Council. One of us (RBGR) was supported by the Netherlands Foundation for Chemical Research (SON) with financial aid from the Netherlands Organization for Scientific Research (NWO). We thank Lilly Tokor for preparation of the AChE, and Alexander Faibusovitch, Clifford Felder, Kurt Giles, Ling Peng and Mia Raves for help, computation and valuable discussions throughout this work. We owe special thanks to Alwyn Jones for suggestions throughout the structure determination and critical comments on this manuscript, and to Bob Sweet, Malcolm Capel and Vivian Stojanoff, at the Brookhaven National Laboratory National Synchrotron Light Source (NSLS), for extraordinary help in collecting the X-ray data.

References

- Harvey, A.L. (1991). *Snake Toxins*. Pergamon, New York.
- Chang, C.C. & Lee, C.Y. (1963). Isolation of neurotoxins from the venom of *Bungarus multicinctus* and their modes of neuromuscular blocking action. *Arch. Int. Pharmacodyn.* **144**, 241–257.
- Libelius, R., Eaker, D. & Karlsson, E. (1975). Further studies on the binding properties of cobra neurotoxin to cholinergic receptors in mouse skeletal muscle. *J. Neural Transm.* **37**, 165–174.
- Changeux, J.-P., Kasai, M. & Lee, C.Y. (1970). The use of a snake venom toxin to characterize the cholinergic receptor protein. *Proc. Natl. Acad. Sci. USA* **67**, 1241–1247.
- Albrand, J.-P., Blackledge, M.J., Pascaud, F., Hollecker, M. & Marion, D. (1995). NMR and restrained molecular dynamics study of the three-dimensional solution structure of toxin FS2, a specific blocker of the L-type calcium channel, isolated from black mamba venom. *Biochemistry* **34**, 5923–5937.
- Ségalas, I., *et al.*, & Toma, F. (1995). Solution structure of a green mamba toxin that activates muscarinic acetylcholine-receptors, as studied by nuclear-magnetic-resonance and molecular modeling. *Biochemistry* **34**, 1248–1260.
- Cerveňansky, C., Dajas, F., Harvey, A.L. & Karlsson, E. (1991). Fasciculins, anticholinesterase toxins from mamba venoms: biochemistry and pharmacology. In *Snake Toxins*. (Harvey, A.L., ed), pp. 131–164, Pergamon, New York.
- le Du, M.H., Marchot, P., Bougis, P.E. & Fontecilla-Camps, J.C. (1992). 1.9-Å resolution structure of fasciculin 1, an anti-acetylcholinesterase toxin from green mamba snake venom. *J. Biol. Chem.* **267**, 22122–22130.
- Wonnacott, S.M. & Dajas, F. (1994). Neurotoxins: nature's untapped bounty. *Trends Pharm. Sci.* **15**, 1–3.
- Barnard, E.A. (1974). Neuromuscular transmission — enzymatic destruction of acetylcholine. In *The Peripheral Nervous System*. (Hubbard, J.I., ed), pp. 201–224, Plenum Press, New York.
- Quinn, D.M. (1987). Acetylcholinesterase: enzyme structure, reaction dynamics, and virtual transition states. *Chem. Rev.* **87**, 955–975.
- Sussman, J.L., *et al.*, & Silman, I. (1991). Atomic structure of acetylcholinesterase from *Torpedo californica*: a prototypic acetylcholine-binding protein. *Science* **253**, 872–879.
- Nolte, H.-J., Rosenberry, T.L. & Neumann, E. (1980). Effective charge on acetylcholinesterase active sites determined from the ionic strength dependence of association rate constants with cationic ligands. *Biochemistry* **19**, 3705–3711.
- Harel, M., *et al.*, & Sussman, J.L. (1993). Quaternary ligand binding to aromatic residues in the active-site gorge of acetylcholinesterase. *Proc. Natl. Acad. Sci. USA* **90**, 9031–9035.

15. Harel, M., Quinn, D.M., Nair, H.K., Silman, I. & Sussman, J.L. (1995). The X-ray structure of a transition state analog complex reveals the molecular origins of the catalytic power and substrate specificity of acetylcholinesterase. *J. Am. Chem. Soc.*, in press.
16. Sussman, J.L. & Silman, I. (1992). Acetylcholinesterase: structure and use as a model for specific cation-protein interactions. *Curr. Opin. Struct. Biol.* **2**, 721-729.
17. Bergmann, F., Wilson, I.B. & Nachmansohn, D. (1950). The inhibitory effect of stilbamidine, curare and related compounds and its relationship to the active groups of acetylcholine esterase. Action of stilbamidine upon nerve impulse conduction. *Biochim. Biophys. Acta* **6**, 217-224.
18. Taylor, P. & Lappi, S. (1975). Interaction of fluorescence probes with acetylcholinesterase. The site and specificity of propidium. *Biochemistry* **14**, 1989-1997.
19. Harel, M., et al., & Silman, I. (1992). Conversion of acetylcholinesterase to butyrylcholinesterase: modeling and mutagenesis. *Proc. Natl. Acad. Sci. USA* **89**, 10827-10831.
20. Ripoll, D.R., Faerman, C.H., Axelsen, P., Silman, I. & Sussman, J.L. (1993). An electrostatic mechanism of substrate guidance down the aromatic gorge of acetylcholinesterase. *Proc. Natl. Acad. Sci. USA* **90**, 5128-5132.
21. Shafferman, A., et al., & Velan, B. (1994). Electrostatic attraction by surface charge does not contribute to the catalytic efficiency of acetylcholinesterase. *EMBO J.* **13**, 3448-3455.
22. Antosiewicz, J., McCammon, J.A., Wlodek, S.T. & Gilson, M.K. (1995). Simulation of charge-mutant acetylcholinesterases. *Biochemistry* **34**, 4211-4219.
23. Ripoll, D.R., Faerman, C.H., Gillilan, R., Silman, I. & Sussman, J.L. (1995). Electrostatic properties of human acetylcholinesterase. In *Enzymes of the Cholinesterase Family*. (Balasubramanian, A.L., Doctor, B.P., Taylor, P. & Quinn, D.M., eds), Plenum Press, New York, in press.
24. Karlsson, E., Mbugua, P.M. & Rodriguez-Iturralde, D. (1984). Fasciculin, anticholinesterase toxins from the venom of the green mamba *Dendroaspis angusticeps*. *J. Physiol.* **79**, 232-240.
25. Cerveñansky, C., Engström, Å. & Karlsson, E. (1994). Study of structure-activity relationship of fasciculin by acetylation of amino groups. *Biochim. Biophys. Acta* **1199**, 1-5.
26. le Du, M.H., Housset, D., Marchot, P., Bougis, P.E., Navaza, J. & Fontecilla-Camps, J.C. (1995). Crystal structure of fasciculin 2 from mamba snake venom: evidence for unusual loop flexibility. *Acta Cryst. D*, in press.
27. Marchot, P., Khelif, A., Ji, Y.H., Mansuelle, P. & Bougis, P.E. (1993). Binding of ¹²⁵I-fasciculin to rat brain acetylcholinesterase. The complex still binds diisopropyl fluorophosphate. *J. Biol. Chem.* **268**, 12458-12467.
28. Eastman, J., Wilson, E.J., Cerveñansky, C. & Rosenberry, T.L. (1995). Fasciculin 2 binds to the peripheral site on acetylcholinesterase and inhibits substrate hydrolysis by slowing a step involving proton transfer during enzyme acylation. *J. Biol. Chem.* **270**, 19694-19701.
29. Radic, Z., Quinn, D.M., Vellom, D.C., Camp, S. & Taylor, P. (1995). Allosteric control of acetylcholinesterase catalysis by fasciculin. *J. Biol. Chem.* **270**, 20391-20399.
30. Cerveñansky, C., Engström, Å. & Karlsson, E. (1995). Role of arginine residues for the activity of fasciculin. *Eur. J. Biochem.* **229**, 270-275.
31. Durán, R., Cerveñansky, C., Dajas, F. & Tipton, K.F. (1994). Fasciculin inhibition of AChE is prevented by chemical modification of the enzyme at a peripheral site. *Biochim. Biophys. Acta* **1201**, 381-388.
32. Radic, Z., Durán, R., Vellom, D.C., Li, Y., Cerveñansky, C. & Taylor, P. (1994). Site of fasciculin interaction with acetylcholinesterase. *J. Biol. Chem.* **269**, 11233-11239.
33. van den Born, H.K.L., Radic, Z., Marchot, P., Taylor, P. & Tsigelny, I. (1995). Theoretical analysis of the structure of the peptide fasciculin and its docking to acetylcholinesterase. *Protein Sci.* **4**, 703-713.
34. Massoulié, J., et al., & Taylor, P. (1992). Recommendations for nomenclature in cholinesterases. In *Multidisciplinary Approaches to Cholinesterase Functions*. (Shafferman, A. & Velan, B., eds), pp. 285-288, Plenum Press, New York.
35. Janin, J. & Chothia, C. (1990). The structure of protein-protein recognition sites. *J. Biol. Chem.* **265**, 16027-16030.
36. Axelsen, P.H., Harel, M., Silman, I. & Sussman, J.L. (1994). Structure and dynamics of the active site gorge of acetylcholinesterase: synergistic use of molecular dynamics simulation and X-ray crystallography. *Protein Sci.* **3**, 188-197.
37. Radic, Z., Pickering, N.A., Vellom, D.C., Camp, S. & Taylor, P. (1993). Three distinct domains in the cholinesterase molecule confer selectivity for acetylcholinesterase and butyrylcholinesterase. *Biochemistry* **32**, 12074-12084.
38. Vellom, D.C., Radic, Z., Li, Y., Pickering, N.A., Camp, S. & Taylor, P. (1993). Amino acid residues controlling acetylcholinesterase and butyrylcholinesterase specificity. *Biochemistry* **32**, 12-17.
39. Eichler, J., Anselmet, A., Sussman, J.L., Massoulié, J. & Silman, I. (1994). Differential effects of 'peripheral' site ligands on *Torpedo* and chicken acetylcholinesterase. *Mol. Pharmacol.* **45**, 335-340.
40. Barak, D., et al., & Shafferman, A. (1994). Acetylcholinesterase peripheral anionic site degeneracy conferred by amino acid arrays sharing a common core. *J. Biol. Chem.* **264**, 6296-6305.
41. Hall, L.M. & Spierer, P. (1986). The Ace locus of *Drosophila melanogaster*: structural gene for acetylcholinesterase with an unusual 5' leader. *EMBO J.* **5**, 2949-2954.
42. Tan, R.C., Truong, T.N., McCammon, J.A. & Sussman, J.L. (1993). Acetylcholinesterase: electrostatic steering increases the rate of ligand binding. *Biochemistry* **32**, 401-403.
43. Nicholls, A. (1992). *GRASP: Graphical Representation and Analysis of Surface Properties*. Dept. of Biochemistry and Molecular Biophysics, Columbia University, New York.
44. Honig, B.H. & Nicholls, A. (1995). Classical electrostatics in biology and Chemistry. *Science* **268**, 1144-1149.
45. Cygler, M., et al., & Doctor, B.P. (1993). Relationship between sequence conservation and three-dimensional structure in a large family of esterases, lipases, and related proteins. *Protein Sci.* **2**, 366-382.
46. Ollis, D.L., et al., & Goldman, A. (1992). The α/β hydrolase fold. *Protein Eng.* **5**, 197-211.
47. Nair, H.K., Lee, K. & Quinn, D.M. (1993). *m*-(*N,N,N*-trimethylammonio)trifluoroacetophenone: a femtomolar inhibitor of acetylcholinesterase. *J. Am. Chem. Soc.* **115**, 9939-9941.
48. Grochulski, P., Li, Y., Schrag, J.D. & Cygler, M. (1994). Two conformational states of *Candida rugosa* lipase. *Protein Sci.* **3**, 82-91.
49. Gilson, M.K., et al., & Sussman, J.L. (1994). Open 'back door' in a molecular dynamics simulation of acetylcholinesterase. *Science* **263**, 1276-1278.
50. Otwinowski, Z. (1993). Oscillation data reduction program. In *Proceedings of the CCP4 Study Weekend: 'Data Collection and Processing'*. (Sawyer, L., Isaacs, N. & Bailey, S., eds), pp. 56-62, SERC Daresbury Laboratory, Warrington, UK.
51. Rossmann, M.G. (1972). The molecular replacement method. In *A Collection of Papers on the Use of Non-Crystallographic Symmetry*. Gordon and Breach Science Publishers, New York.
52. Navaza, J. (1994). AMORE — an automated procedure for molecular replacement. *Acta Cryst. D* **50**, 157-163.
53. Brünger, A.T. (1992). *X-PLOR Version 3.1. A System for Crystallography and NMR*. Yale University Press, New Haven and London.
54. Jones, T.A., Zou, J.-Y., Cowan, S.W. & Kjeldgaard, M. (1991). Improved methods for the building of protein models in electron density maps and the location of errors in these models. *Acta Cryst. A* **47**, 110-119.
55. Collaborative Computational Project Number 4 (1994). The CCP4 suite: programs for protein crystallography. *Acta Cryst. D* **50**, 760-763.
56. Kleywegt, G.J. & Jones, T.A. (1995). Where freedom is given, liberties are taken. *Structure* **3**, 535-540.
57. Brünger, A.T., Krukowski, A. & Erickson, J. (1990). Slow-cooling protocols for crystallographic refinement by simulated annealing. *Acta Cryst. A* **46**, 585-593.
58. Brünger, A.T. (1992). Free R value: a novel statistical quantity for assessing the accuracy of crystal structures. *Nature* **355**, 472-475.
59. Kleywegt, G.J. & Jones, T.A. (1995). Efficient rebuilding of protein structures. *Acta Cryst. D*, in press.
60. Kleywegt, G.J. & Jones, T.A. (1994). Halloween...masks and bones. In *From First Map to Final Model*. (Bailey, S., Hubbard, R. & Waller, D.A., eds), pp. 59-66, SERC Daresbury Laboratory, Warrington, UK.
61. Engh, R.A. & Huber, R. (1991). Accurate bond and angle parameters for X-ray protein-structure refinement. *Acta Cryst. A* **47**, 392-400.
62. Ramachandran, C. & Ramakrishnan, C.N. (1965). Stereochemical criteria for polypeptide and protein chain conformations. II. Allowed conformations for a pair of peptide units. *Biophys. J.* **5**, 909-933.
63. Bernstein, F.C., et al., & Tasumi, M. (1977). The protein data bank: a computer-based archival file for macromolecular structures. *J. Mol. Biol.* **112**, 535-542.
64. Laskowski, R.A., MacArthur, M.W., Moss, D. & Thornton, J.M. (1993). PROCHECK: a program to check the stereochemical quality of protein structures. *J. Appl. Cryst.* **26**, 283-291.
65. Vriend, G.A. & Sander, C. (1993). Quality control of protein models: directional atomic contact analysis. *J. Appl. Cryst.* **26**, 47-60.
66. Kleywegt, G.J. & Jones, T.A. (1994). Detection, delineation, measurement and display of cavities in macromolecular structures. *Acta Cryst. D* **50**, 178-185.
67. Kraulis, P.J. (1991). MOLSCRIPT: a program to produce both detailed and schematic plots of protein structure. *J. Appl. Cryst.* **24**, 946-950.
68. Bairoch, A. & Boeckmann, B. (1994). The SWISS-PROT protein sequence data bank: current status. *Nucleic Acids Res.* **22**, 3578-3580.
69. Feng, D.-F. & Doolittle, R.F. (1987). Progressive sequence alignment as a prerequisite to correct phylogenetic trees. *J. Mol. Evol.* **25**, 351-360.
70. Cousin, X., Hotelier, T., Lievin, P., Toutant, J.-P. & Chatonnet, A. (1995). A CHOLINESTERASE GENES SERVER (ESTHER): a data base of cholinesterase-related sequences for multiple alignments, phylogenetic relationships, mutations and structural data retrieval. *Nucleic Acids Res.*, in press.

Received: 13 Oct 1995; revisions requested: 24 Oct 1995;
revisions received: 1 Nov 1995. Accepted: 1 Nov 1995.